

Effects of microscopic strain distribution on $\text{Ga}_{1-x}\text{In}_x\text{As}$ quantum wires grown by strain-induced lateral ordering

Liang-Xin Li, Jingze Sun and Yia-Chung Chang

Department of Physics and Materials Research Laboratory

University of Illinois at Urbana-Champaign, Urbana, Illinois 61801

(November 15, 2018)

Band structures and optical matrix elements of quantum wires (QWR's) made of short-period superlattices (SPS) with strain-induced lateral ordering (SILO) are investigated theoretically via an effective bond-orbital model (EBOM) combined with a valence-force field (VFF) model. Valence-band anisotropy, band mixing, and effects due to local strain distribution at the atomistic level are all taken into account. In particular, $\text{Ga}_{1-x}\text{In}_x\text{As}$ QWR's grown by SILO process are considered. A VFF model is used to find the equilibrium atomic positions in the SILO QWR structure by minimizing the lattice energy. The strain tensor at each atomic (In or Ga) site is then obtained and included in the calculation of electronic states and optical properties. It is found that different local arrangement of atoms leads to very different strain distribution, which in term alters the optical properties. In particular, we found that the optical anisotropy can be reversed due to the change in shear strain caused by the inter-change of atomic positions. Good agreement with the existing experimental data on band gap and optical anisotropy can be obtained when a 2D alloy structure with lateral composition modulation in the InAs/GaAs interface planes of the SPS is used. Our studies revealed the possibility of "shear-strain engineering" in SILO QWR light-emitting devices to achieve desired optical anisotropy.

I. INTRODUCTION

Optical properties of III-V semiconductor nanostructures have attracted a great deal of interest, as they are important for applications in optical communications that involve switching, amplification, and signal processing. $\text{Ga}_x\text{In}_{1-x}\text{As}$ and $\text{Ga}_x\text{In}_{1-x}\text{P}$ are among the most important ternary III-V compound semiconductors. $\text{Ga}_x\text{In}_{1-x}\text{As}$ in particular has band gaps covering both the 1.3 and 1.55 μm range, which are the preferred wavelengths in long distance fiber communications[1-3]. However, long-wavelength photonic devices based on lattice-matched $\text{Ga}_{0.47}\text{In}_{0.53}\text{As}/\text{InP}$ heterostructures suffer from strong Auger recombination and intervalence band absorption processes[4-7]. Recently, to improve the performance of long-wavelength semiconductor lasers, long wavelength ($\sim 1.55\mu\text{m}$) $\text{Ga}_x\text{In}_{1-x}\text{As}$ quantum-wire (QWR) lasers have been grown by a single step molecular beam epitaxy technique[1].

An important optical property is the change in the emission of light (in energy, polarization, and intensity) that results from phase-space filling of carriers in one- and two-dimensionally confined systems, i.e., As the dimensionality of the quantum confinement increases from one dimension (1D) to 2D, the narrowing of the density of states will exhibit a lower excitation threshold for phase-space filling, thereby, yielding potentially enhanced optical effects. It is found that the QWR laser structures are a promising candidate for optical communication device because of the many predicted benefits, such as higher gain, reduced temperature sensitivity, higher modulation bandwidths, and narrower spectral linewidths[2].

The fabrication of quantum wires via the strain-induced lateral-layer ordering (SILO) process starts with the growth of short-period superlattices (SPS) [e.g. $(\text{GaAs})_2/(\text{InAs})_{2.2}$] along the [001] direction. The excess fractional InAs layer leads to stripe-like islands during the MBE growth. The continued growth of $(\text{GaAs})_2/(\text{InAs})_2$ SPS on top of this surface will lead to spatial separation of Ga-rich stripes and In-rich stripes due to the effect of strain potential.[1,2] Thus, a strain-induced lateral ordering occurs and a quantum wire heterostructure can then be created by simply utilizing this SPS structure with lateral composition modulation as the quantum well region in a conventional quantum heterostructure. In the experiment performed by Chou et al[1] and Tang et al[2], the QWR active region is created *in situ* by the SILO process within the $(\text{GaAs})_2/(\text{InAs})_2$ SPS regions. The SILO process generates a strong Ga/In lateral composition modulation and creates Ga-rich $\text{Ga}_x\text{In}_{1-x}\text{As}$ lateral QWs in the [110] direction. By sandwiching the composition modulated layer between $\text{Al}_{0.24}\text{Ga}_{0.24}\text{In}_{0.52}\text{As}$ barrier layers, a strained QWR heterostructure is formed[1,2]. Besides the self-assembled lateral ordering, it is believed that the strain also plays a key role[2] in the temperature stability and optical anisotropy for the QWR laser structure. Recent studies indicate that the use of the strained-layer quantum wire heterostructure has advantages of high-quality interfaces and band-gap tuning which are independent of the lattice constant of the constituent materials[3,4]. Furthermore, much work has been undertaken which predicts that by using strained-layer superlattice to form the active region of a quantum-wire laser, the threshold current can be decreased by one order of magnitude, and the optical loss due to intervalence-band absorption and

Auger recombination will also be greatly reduced[1,2,5-8]. Also, the temperature sensitivity is reduced by an order of magnitude compared with strain-free structures[2]. A typical temperature sensitivity of the lasing wavelength is ($\sim 5\text{\AA}/^{\circ}\text{C}$) for the usual GaInAs/InP lasers. By using a distributed-feedback structure, the temperature dependence of the lasing wavelength is reduced to $1\text{\AA}/^{\circ}\text{C}$ [2]. With this strained GaInAs QWR, the dependence is smaller than $0.1\text{\AA}/^{\circ}\text{C}$ [2]. It should be an important improvement on the current technology in fabricating the long wavelength lasers for fiber communication. In this paper we study the effects of multi-axial strain on the electronic and optical properties of the QWR structures grown via the SILO process. Through this study, we can gain a better understanding of the strain engineering of QWR structures suitable for the application of fiber-optical communication.

In a previous paper[9], we performed theoretical calculations of the optical properties of SILO QWR's within the virtual crystal approximation in which the SPS region is modeled by a $\text{Ga}_x\text{In}_{1-x}\text{As}$ alloy with a lateral modulation of the composition x . Although our calculation can explain the QWR band gap and optical anisotropy approximately, it does not take into account the detailed SPS structure and the microscopic strain distribution. The understanding of these effects is important if one wish to have a full design capability of the SILO QWR optoelectronic devices.

In the present paper, we consider two possible local atomic arrangements with SPS structure in the SILO quantum wires and examine the effects of the microscopic strain distribution on the electronic and optical properties. The QWR model structures considered in the present paper are depicted in Fig. 1. Both model structures start with a quantum well nanostructure in which the supercell consists of 8 stacks of (001) $(\text{GaAs})_2/(\text{InAs})_2$ SPS with a total thickness of $\approx 100\text{\AA}$ (quantum well region) followed by a $\text{Al}_{0.24}\text{Ga}_{0.24}\text{In}_{0.52}\text{As}$ layer (barrier region) with thickness $\approx 60\text{\AA}$ (20 diatomic layers). In the first QWR model structure (a), the strain-induced lateral ordering is modeled by interchanging a segment of 29 Ga atoms in the right half of the first row in the SPS (each row in the SPS consists of 72 atoms along the [110] direction such that the period is around 300\AA) with a segment of 29 In atoms in the left half of the third row. [see Fig. 1(a)] This structure is an idealized model of a SILO QWR which starts with a growth of $(\text{GaAs})_2/(\text{InAs})_{2,2}$ SPS. It is assumed that during growth an extra 0.4 monolayer of In atoms on the surface form stripe-like islands aligned along the $[\bar{1}\bar{1}0]$ direction [corresponding to the segment of 29 In atoms in the first row of Fig. 1(a)], which serves as a seed structure for the formation of the SILO QWR. The deposition of two more GaAs monolayers leaves extra 0.4 monolayer of Ga atoms on the surface, which again form stripe-like islands [corresponding to the segment of 29 Ga atoms in the third row of Fig. 1(a)]. Due to the strain potential, the Ga stripes are spatially separated from the In stripes buried two monolayers beneath. Thus, the continued growth of $(\text{GaAs})_2/(\text{InAs})_2$ SPS on top of the seed structure will lead to a SILO QWR structure shown in Fig. 1(a).

In the second QWR model structure (b), we assume that the extra 0.4 monolayer of In atoms on the surface of the seed structure mix randomly with the newly deposited Ga atoms during growth so as to form a composition modulated 2D alloy structure on the surface. The In composition x is assumed to vary in the [110] direction (or y' direction) according to the relation [see Fig. 1(c)]

$$x = \begin{cases} 0 & \text{for } b < y' < L_1 - b \\ 0.4 + 0.4 \sin[\pi(y' - L_1)/2b] & \text{for } L_1 - b < y' < L_1 + b \\ 0.8 & \text{for } L_1 + b < y' < L - b \\ 0.4 - 0.4 \sin[\pi(y' - L)/2b] & \text{for } y' < b \text{ or } L - b < y', \end{cases} \quad (1)$$

where $2b$ denotes the width of composition grading, L_1 is the length of Ga-rich region in the QWR, and L is the period of the lateral modulation in the $[110]$ direction. Here we use $b = 6a_{[110]} \approx 20\text{\AA}$ (??).

In both model structures, we can divide the SILO QWR into two regions with the left half being Ga rich and the right half In rich. The average Ga (In) mole fraction in the Ga (In)-rich region is 0.7 (0.3). Alternatively, we can divide the first structure into three regions which include $(\text{InAs})_1(\text{GaAs})_3$, $(\text{InAs})_2(\text{GaAs})_2$, and $(\text{InAs})_3(\text{GaAs})_1$ SPS's with the In mole fraction changes abruptly between boundaries of the three regions. In the second structure, the In mole fraction for the whole QWR varies continuously between 0.3 and 0.7 for y' changing from the Ga-rich region to the In-rich region.

A valence force field (VFF) model[10-12] is used to find the equilibrium atomic positions in the SILO QWR structure by minimizing the lattice energy. The strain tensor at each atomic (In or Ga) site is then obtained by calculating the local distortion of chemical bonds. We found that different local arrangement of atoms can lead to very different strain distribution. In particular, the shear strain can change substantially from structure 1 (with abrupt change in In composition) to structure 2 (with gradual change in In composition). Furthermore, we found that the optical anisotropy can be reversed due to the change in the strength of the shear strain caused by the intermixing of In and Ga atoms. We found that both structures give band gaps close to experimental value. However, only the second structure gives good agreement with the published experimental data[1,2] on both band gap and optical anisotropy, indicating that random mixing of In and Ga atoms on the growth surface when the island structure is present best matches the experimental situation.

II. THEORETICAL APPROACH

The method used in this paper for calculating the strained QWR band structure is based on the effective bond-orbital model (EBOM). A detailed description of this method has been published elsewhere[13,14]. EBOM is a tight binding-like model with minimum set of localized basis (the bonding or anti-bonding orbitals). The interaction and optical parameters are obtained by a correspondence with the $\mathbf{k} \cdot \mathbf{p}$ theory, which can be cast into analytic forms. Thus, the model can be viewed as a spatially discretized version of the $\mathbf{k} \cdot \mathbf{p}$ method, while retaining the virtues of LCAO (linear combination of atomic orbitals) method. The $\mathbf{k} \cdot \mathbf{p}$ model is the most popular one for treating electronic structures of semiconductor quantum wells or superlattices. However, when applied to complex structures such as SILO quantum wires[1-4] or self-assembled quantum dots[10,15], the method becomes very cumbersome if one wish to

implement the correct boundary conditions that take into account the differences in $\mathbf{k} \cdot \mathbf{p}$ band parameters for different materials involved. EBOM is free of this problem, since different material parameters are used at different atomic sites in a natural way. For simple structures, when both EBOM and $\mathbf{k} \cdot \mathbf{p}$ model are equally applicable, the results obtained are essentially identical.[13]

The optical matrix elements for the QWR states are computed in terms of elementary optical matrix elements between the valence-band bond orbitals and the conduction-band orbitals. The present calculation includes the coupling of the four spin-3/2 valence bands and the two spin-1/2 conduction bands closest to the band edges. Thus, it is equivalent to a 6-band $\mathbf{k} \cdot \mathbf{p}$ model. For our systems studied here, the band-edge properties are relatively unaffected by the split-off band due to the large spin-orbit splitting as discussed in our previous paper[9]. Hence, the split-off bands are ignored here. The bond-orbitals for the GaAs and InAs needed in the expansion of the superlattice states contain the following: four valence-band bond orbitals per bulk unit cell, which are p-like orbitals coupled with the spin to form orbitals with total angular momentum $J=3/2$ plus two conduction-band bond orbitals with $J=1/2$. They are written as

$$|\mathbf{R}, u_{JM} \rangle = \sum_{\alpha, \sigma} C(\alpha, \sigma, J, M) |\vec{R}, \alpha \rangle \psi_{\sigma}, \quad (2)$$

where $J = 1/2$ and $3/2$ for the conduction and valence bands, respectively, and $M = -J, \dots, J$, ψ_{σ} , designates the electron spinor ($\sigma=1/2, -1/2$), and $|\mathbf{R}, \alpha \rangle$ denote an α -like ($\alpha = s, x, y, z$) bond orbital, located at unit cell \mathbf{R} . $C(\alpha, \sigma, J, M)$ are the coupling coefficients obtainable by group theory. All these bond orbitals are assumed to be sufficiently localized so that the interaction between orbitals separated farther than the nearest-neighbor distance can be ignored.

The effect of strain is included by adding a strain Hamiltonian H^{st} to the EBOM Hamiltonian[14]. The matrix elements of H^{st} in the bond-orbital basis can be obtained by the deformation-potential theory of Bir and Pikus[16]. We use the valence-force field (VFF) model of Keating and Martin[11,12] to calculate the microscopic strain distribution. This model has been shown to be successful in fitting and predicting the elastic constants of elastic continuum theory, calculating strain distribution in a quantum well, and determining the atomic structure of III-V alloys. It was also used in the calculation of the strain distribution in self-assembled quantum dots.[10] The VFF model is a microscopic theory which includes bond stretching and bond bending, and avoids the potential failure of elastic continuum theory in the atomically thin limit. The total energy of the lattice is taken as

$$V = \frac{1}{4} \sum_{ij} \frac{3}{4} \alpha_{ij} (d_{ij}^2 - d_{0,ij}^2)^2 / d_{0,ij}^2 + \frac{1}{2} \sum_i \sum_{j \neq k} \frac{3}{4} \beta_{ijk} (\vec{d}_{ij} \cdot \vec{d}_{ik} + d_{0,ij} d_{0,ik} / 3)^2 / d_{0,ij} d_{0,ik} \quad (3)$$

where i runs over all the atomic sites, j, k run over the nearest-neighbor sites of i , \vec{d}_{ij} is the vector joining the sites i and j , d_{ij} is the length of the bond, $d_{0,ij}$ is the corresponding equilibrium length in the binary constituents, and α_{ij} and β_{ijk} are the bond stretching and bond bending constants, respectively. α and β are from Martin's calculations.[11]

For the bond-bending parameter β of In-As-Ga, we take $\beta_{ijk} = \sqrt{\beta[ij]\beta[ik]}$ following Ref. [17].

To find the strain tensor in the *InAs/GaAs* SILO QWR, we start from ideal atomic positions and minimize the system energy using the Hamiltonian given above. Minimization of the total energy requires one to solve a set of coupled equations with $3N$ variables, where N is the total number of atoms. Direct solution of these equations is impractical in our case, since the system contains more than 6,000 atoms. We use an approach taken by several authors which has been shown to be quite efficient. In the beginning of the simulation all the atoms are placed on the InP lattice, we allow atoms to deviate from this starting positions and use periodic boundary conditions in the plane perpendicular to the growth direction, while keeping atoms in the planes outside the SPS region at their ideal atomic positions for a InP lattice (since the SILO QWR is grown epitaxially on the InP substrate). In each iteration, only one atomic position is displaced and other atom positions are held fixed. The direction of the displacement of atom i is determined according to the force $f_i = \partial V / \partial x_i$ acting on it. All atoms are displaced in sequence. the whole sequence is repeated until the forces acting on all atoms become zero at which point the system energy is a minimum. Once the positions of all the atoms are known, the strain distribution is obtained through the strain tensor calculated according to the method described in Ref. [18].

Let R^0 be the position matrix without strain:

$$R^0 = \begin{pmatrix} R_{12x}^0 & R_{23x}^0 & R_{34x}^0 \\ R_{12y}^0 & R_{23y}^0 & R_{34y}^0 \\ R_{12z}^0 & R_{23z}^0 & R_{34z}^0 \end{pmatrix},$$

where $\mathbf{R}_{ij}^0 = \mathbf{R}_j^0 - \mathbf{R}_i^0$; $i, j = 1, 4$ and \mathbf{R}_i^0 ($i = 1, 4$) denote positions of four As atoms surrounding a Ga or In atom. Here we choose $\mathbf{R}_{12}^0 = (1, -1, 0)a/2$, $\mathbf{R}_{23}^0 = (-1, 0, -1)a/2$, and $\mathbf{R}_{34}^0 = (1, 1, 0)a/2$. a is the lattice constant of GaAs or InAs, depending on the site. Let R be the corresponding position matrix with strain. It was shown in Ref. [18] that the strain tensor is given by

$$\epsilon = R * R_0^{-1} - 1. \quad (4)$$

After getting the strain tensor, the strain Hamiltonian is given by Bir and Pikus[16]

$$H^{st} = \begin{pmatrix} -\Delta V_H + D_1 & \sqrt{3}de_{xy} & \sqrt{3}de_{xz} \\ \sqrt{3}de_{xy} & -\Delta V_H + D_2 & \sqrt{3}de_{yz} \\ \sqrt{3}de_{xz} & \sqrt{3}de_{yz} & -\Delta V_H + D_3 \end{pmatrix}, \quad (5)$$

where $e_{ij} = (\epsilon_{ij} + \epsilon_{ji})/2$, and

$$\Delta V_H = (a_1 + a_2)(\epsilon_{xx} + \epsilon_{yy} + \epsilon_{zz}), \quad D_1 = b(2\epsilon_{xx} - \epsilon_{yy} - \epsilon_{zz}), \quad D_2 = b(2\epsilon_{yy} - \epsilon_{xx} - \epsilon_{zz}), \quad D_3 = b(2\epsilon_{zz} - \epsilon_{yy} - \epsilon_{xx}),$$

The strain potential on the s states is given by

$$\Delta V_c = c_1(\epsilon_{xx} + \epsilon_{yy} + \epsilon_{zz}),$$

The strain Hamiltonian in the bond-orbital basis $|JM\rangle$ can be easily found by using the coupling constants[13], i.e,

$$\langle JM|H^{st}|J'M'\rangle = \sum_{\alpha,\alpha',\sigma} C(\alpha,\sigma;J,M)^* C(\alpha',\sigma;J',M') H_{\alpha\alpha'}^{st} \quad (6)$$

The elastic constants C_{12} and C_{11} for GaAs, InAs and AlAs can be found in Ref. [18,19]. The deformation potentials a_1, a_2, b, c_1, d can be found in Ref.[20,21]. The linear interpolation and virtual crystal approximations used to obtain the corresponding parameters for the barrier material ($\text{Al}_{0.24}\text{Ga}_{0.24}\text{In}_{0.52}\text{As}$).

The above strain Hamiltonian is derived locally for the each cation atom in the SILO QWR considered. To calculate the electronic states of the SILO QWR, we first construct a zeroth-order Hamiltonian for a superlattice structure which contains in each period 8 stacks of (001) $(\text{GaAs})_2/(\text{InAs})_2$ SPS layers (with a total thickness around 100 Å) and 20 diatomic layers of $\text{Al}_{0.24}\text{Ga}_{0.24}\text{In}_{0.52}\text{As}$ (with thickness around 60 Å). So, the superlattice unit cell for the zeroth-order model contains 52 diatomic layers. The appropriate strain Hamiltonian for the the $(\text{GaAs})_2/(\text{InAs})_2$ SPS on InP is also included.

The eigen-states for the zero-th order Hamiltonian for different values of k_2 (separated by the SL reciprocal lattice vectors in the [110] direction) are then used as the basis for calculating the SILO QWR electronic states. The difference in the Hamiltonian (including strain effects) caused by the intermixing of Ga and In atoms at the interfaces is then added to the zeroth-order Hamiltonian, and the electronic states of the full Hamiltonian is solved by diagonalizing the Hamiltonian matrix defined within a truncated set of eigen-states of the zeroth-order Hamiltonian. A total of ~ 300 eigenstates of the zero-th order Hamiltonian (with 21 different k_{110} points) were used in the expansion. The subbands closest to the band edge are converged to within 0.1 meV.

III. RESULTS AND DISCUSSIONS

A. Strain distributions

In this section we discuss strain distributions in two QWR model structures as described in section I. In both structures composition modulation is along the y' ([110]) direction. In structure 1 atomic species are unchanged along x' ($[1,\bar{1},0]$), while in structure 2 we have an 2D $\text{In}_x\text{Ga}_{1-x}\text{As}$ alloy with the composition x varying as a function of y' . The diagonal and shear strains of structure 1 are shown in Figs. 2 and 3, respectively. For best illustration, we show diagonal strains in a rotated frame, in which x' is $[1,\bar{1},0]$, y' is [110], and z' is [001]. Shear strains are shown in the original Cartesian coordinates.

Since the atomic species does not change along x' , the x' coordinate of all atoms are very close to the original values pinned by the substrate (InP), thus $\epsilon_{x'x'}$ (solid lines) are essentially constants along y' in regions where atomic species are same. For example, Layer 2 contains all In atoms, and $\epsilon_{x'x'}$ is constant with a value equal to $(a_{\text{InAs}} - a_{\text{InP}})/a_{\text{InAs}}$. In layer 1, Ga atoms occupy the sites labeled $y=40-68$, and the rest are In atoms. Thus, there is a discrete jump of

$\epsilon_{x'x'}$ from $a_{InP} - a_{InAs}/a_{InAs}$ to $a_{InP} - a_{GaAs}/a_{GaAs}$. In the ideal situation (without lateral relaxation), $\epsilon_{y'y'}$ should be the same as $\epsilon_{x'x'}$ due to symmetry. However, with the lateral modulation as considered here, all Ga(In) atoms tend to shift in a direction so as to reduce the strain in the Ga(In)-rich region, while they shift in the opposite direction in the In(Ga)-rich region. Thus, the magnitude of $\epsilon_{y'y'}$ on Ga(In) sites (dashed lines in Fig. 2) is lower than $\epsilon_{x'x'}$ in Ga(In)-rich region and vice versa in In(Ga)-rich region. On the other hand, the z component strain (dash-dotted lines) tend to compensate the other two components such that the volume of each bulk unit cell is close to that for the unstrained bulk. Thus, we see that $\epsilon_{z'z'}$ has an opposite sign compared to $\epsilon_{x'x'}$ or $\epsilon_{y'y'}$ at all atomic sites.

The difference in $\epsilon_{x'x'}$ and $\epsilon_{y'y'}$ leads to a nonzero shear strain $e_{xy} = (\epsilon_{y'y'} - \epsilon_{x'x'})/2$ in the original coordinates. The shear strain is particularly strong at the interface where the atomic species changes abruptly. (see solid lines in Fig. 3). The other shear strains ϵ_{xz} and ϵ_{yz} (dash-dotted lines) are also quite significant (around 1-2 %) in structure 1. The structure has a mirror plane normal to the x' axis; thus we have $\epsilon_{xz} = \epsilon_{yz}$ here.

To model the alloy structure with composition modulation (structure 2), we use a super-cell which contains 72 atoms in the $[110]$ (y') direction, 36 atoms in the $[\bar{1}\bar{1}0]$ (x') direction and 18 atomic planes along the $[001]$ (z) direction [2 stacks of (2/2) SPS plus one monolayer of GaAs latticed matched to InP]. In the atomic planes which consist of alloy structure, we first determine the In composition at a given y' according to Eq. (1) and then use a random number generator to determine the atomic species along the x' direction. The calculated strain distributions are then averaged over the x' coordinate. The middle four layers are used as the supercell for the SILO QWR structure as shown in Fig. 1(b). Their strain distributions are shown below.

Fig. 4 shows the diagonal strain distributions of the second structures in the rotated coordinates (x', y', z'). Comparing with those in structure 1, strain distributions are quite different in structure 2. Due to the random distribution of In/Ga atoms along x' in the alloy layers, the difference of $\epsilon_{x'x'}$ and $\epsilon_{y'y'}$ is significantly reduced. Since In composition x changes sinusoidally between Ga-rich and In-rich regions in layer 1 (3) $\epsilon_{x'x'}$ and $\epsilon_{y'y'}$ also change gradually from their GaAs (InAs) bulk values to the alloy bulk values. The average values of $\epsilon_{x'x'}$ in layers 1 and 3 are essentially the softened profiles of those shown in Fig. 2 for structure 1, while they remain approximately constant in layers 2 and 4.

Fig. 5 shows the off-diagonal strain distributions of the second structures in the original coordinates. Due to the gradual change of In composition from Ga-rich to In-rich regions, the shear strain is on average five times smaller than its counterpart in structure 1. The largest xy -component shear strain (solid line) is around 0.4%, which occurs near the boundary between Ga-rich and In-rich regions. We show below that the significant difference in shear strains between the two QWR model structures will lead to dramatically different optical properties.

B. Electronic structures

In order to understand the aspect of lateral quantum confinement due to lateral composition modulation and strain, we first examine the band-edge energies of a strained quantum well structure whose well material is the same as the SPS structure appeared in the SILO QWR with a fixed value of y' coordinate. For structure 1 depicted in Fig. 1(a), the

well material consists of 8 stacks $(\text{GaAs})_{2-n}/(\text{InAs})_{2+n}$ SPS with $n = -1, 0, 1$ in different regions of the SILO QWR. In structure 2, the $(\text{GaAs})_{2-n}/(\text{InAs})_{2+n}$ SPS is replaced by a $\text{GaAs}_2/\text{Ga}_{1-x}\text{In}_x\text{As}/\text{InAs}$ ($\text{GaAs}/\text{Ga}_{1-x}\text{In}_x\text{As}/\text{InAs}_2$) SPS in the Ga-rich (In-rich) region of the SILO QWR with x varying as a function of y' according to Eq. (1).

The results for the conduction band minimum and valence band maximum of the above quantum well as functions of y' are shown in Fig. 6 (dashed lines). For comparison, the corresponding band edges for a SPS structure without the $\text{Al}_{0.24}\text{Ga}_{0.24}\text{In}_{0.52}\text{As}$ confining barrier are also shown with (dash-dotted) and without (solid) the effect of strain. The strain Hamiltonian used here is the same as the one used in the SILO QWR at the corresponding y' . All material parameters are chosen the same as in Ref. [9] for temperature at 77K, except that the deformation potentials used here are slightly different. We use $C_1 = -9.3, -4.1, a_1 + a_2 = -2.7, -2.5\text{eV}$ for GaAs and InAs, respectively. These values are within the uncertainties of experimentally determined values[20,21] and they give a better agreement for the band gaps of $(\text{GaAs})_2(\text{InAs})_2$ SPS and SILO QWRs between the calculated and experimental values. The photoluminescence (PL) measurements indicates that the $(\text{GaAs})_2(\text{InAs})_2$ SPS grown on InP substrate has a gap around 0.76 eV.[22] Her we obtain a band gap of 0.76 eV for the $(\text{GaAs})_2(\text{InAs})_2$ SPS (at $y'=36$) and 0.78 eV for 8 stacks (or 100 Å) of $(\text{GaAs})_2(\text{InAs})_2$ SPS sandwiched between $\text{Al}_{0.24}\text{Ga}_{0.24}\text{In}_{0.52}\text{As}$ confining barriers. This is also consistent with the PL measurements on the $(\text{GaAs})_2(\text{InAs})_2/\text{InP}$ multiple quantum wells.[22] As seen in this figure, the strain effect causes a shift of conduction band edge by ~ 0.5 eV (0.4 eV) and valence-band edge by ~ 0.4 eV (0.3 eV) in structure 1 (structure 2). The band-edge profiles shown in this figure suggest that both electrons and holes are confined in the Ga-rich region with a band offset around 0.15 eV for the electron and 0.05 eV for the hole. Both offsets are large enough to give rise to strong lateral confinement for electrons and holes in the Ga-rich region.

Fig. 7 shows the near zone-center valence subband structures of the QWR model structure 1 as depicted in Fig. 1(a). All subbands are two-fold degenerate at the zone center due to the Kramer's degeneracy and they split at finite wave vectors as a result of lack of inversion symmetry in the system. Comparing the band structures in both k_1 ($[\bar{1}\bar{1}0]$) and k_2 ($[110]$) directions, we noticed an apparent anisotropy in the energy dispersion. The dispersions in the k_2 direction for the (confined) valence bands are rather small, indicating strong lateral confinement. The first three pairs of subbands are labeled V1, V2, and V3. They have unusually large energy separations compared with other valence subbands. This is because the first three pairs of subbands represent QWR confined states, whereas the other valence subbands (with energies below -110 meV) are unconfined by the lateral composition modulation. To examine the effects caused by the shear strain, we have also calculated the band structures with the shear strain set to zero. We found that without the shear strain the first pairs of valence subbands (V1) have much larger dispersion along the k_1 direction with an effective masses along $[\bar{1}\bar{1}0]$ about a factor five smaller than the effective mass for the V1 subbands with the shear strain. This indicates that the V1 subband states for the case without shear strain are derived mainly from bond orbitals with x' -character, which leads to stronger overlap between two bond orbitals along the x' direction, hence larger dispersion along k_1 . When the shear strain is present, the character of bond orbitals in the

V1 subband states change from mainly x' -like to predominantly y' -like; thus, the dispersion along k_1 becomes much weaker. This explains the very flat V1 subbands as shown in Fig. 7. Physically, the switching of orbital character in the V1 subbands can be understood as follows. When the shear strain is absent, we have $\epsilon_{x'x'} = \epsilon_{y'y'}$, and the confinement effect in the y' direction pushes down the subband with y' character (which has smaller effective mass in the y' direction), thus leaving the top valence subband (V1) to have [predominantly x' character. On the other hand, with the presence of shear strain as shown in structure 1, we have $\epsilon_{y'y'} > \epsilon_{x'x'}$ in Ga-rich region, and the strain potential forces the y' -like subband to move above the x' -like subband, overcoming the confinement effect. As a result, the V1 subbands become y' -like. The conduction subbands are approximately parabolic as usual with a zone-center subband minimum equal to 716 meV. This gives an energy gap of 791 meV for QWR model structure 1.

Fig. 8 shows the optical matrix elements squared (P^2) for transitions from the highest three pairs of valence subbands to the first pair of conduction subbands. Here P^2 is defined as $\frac{2}{m_0} \sum_{s,s'} | \langle \psi_v | \hat{\epsilon} \cdot \mathbf{p} | \psi_c \rangle |^2$, where ψ_v (ψ_c) denotes a valence (conduction) subband state. The symbol $\sum_{s,s'}$ means a sum over two near degenerate pair of subbands in the initial and final states. $\hat{\epsilon}$ denotes the polarization of light. Here we consider only the x' (along the QWR axis) and y' (perpendicular to the QWR axis) components. As seen in this figure, the C1-V1 transition for y' -polarization (dashed line) is about two times that for the x' -polarization (solid line), indicating an optical anisotropy $((P_{[1\bar{1}0]}^2 - P_{[110]}^2)/(P_{[1\bar{1}0]}^2 + P_{[110]}^2))$ around 0.4. This is consistent with the discussion for valence subband structures shown in Fig. 7, where we concluded that the bond orbitals involved in the V1 subbands are predominantly y' -like. The optical anisotropy for QWR model structure 1 is reversed compared with the optical anisotropy observed in the photoluminescence measurements for most InGaAs SILO QWRs. As pointed out in our previous paper, the lateral confinement in a typical QWR (without shear strain) leads to a positive optical anisotropy[9]. Here we found the opposite result. This apparent "anomaly" is caused by the presence of the strong shear strain (especially the xy component) in the QWR model structure. If we artificially turn off the shear strain, then the normal (positive) optical anisotropy can be resumed. We have studied several other model structures. We found that as long as we maintain an ordered structure along the x' (with the same periodicity as bulk), the lateral modulation in the y' direction is necessarily a sharp transition in In composition, and the structure always has a large shear strain near the boundary where the In composition changes. The fact that most SILO QWRs display a positive optical anisotropy indicating that these structures can not be modeled by a ordered SPS structure as depicted in Fig. 1 (a). On the other hand, there do exist a few SILO QWR samples that display a slightly negative optical anisotropy at 77K[23]. Perhaps, these SILO QWR structures have more abrupt change in In composition along the [110] direction.

Knowing that a positive optical anisotropy can occur in a QWR structure with weak shear strain, we now turn to our model structure 2, in which a gradual lateral modulation in In composition substantially reduces the shear strain (see Fig. 5). The calculated valence subband structures for this QWR model structure are shown in Fig. 9. Comparing this figure with Fig. 7, we find striking differences in band structures for the two QWR model structures.

The first pairs of subbands (labeled V1) in Fig. 9 has much larger dispersion than their counterparts in Fig. 7, and there exists an anti-cross behavior between the first pair of subbands (labeled V1) and the lower subbands (similar to the LH1-HH2 anti-crossing pattern typically appeared in III-V quantum wells[24,25]) near $k_1 = 0.02(2\pi/a)$ in Fig. 9. This anti-crossing pattern is missing in Fig. 7 for QWR model structure 1. Again, the presence of the strong shear strain in the QWR structure is responsible for this difference. By turning off the shear strain artificially in QWR model structure 1, we found that the dispersion of the V1 subbands become similar to that shown in Fig. 9 with an anti-crossing pattern. The conduction band minimum (not shown) is 676 meV for QWR model structure 2. This gives rise to a band gap of 767 meV, which is very good agreement with the experimental results for InGaAs SILO QWR with similar specification.

Fig. 10 shows the squared optical matrix elements (P^2) versus wave vectors of QWR model structure 2 for transitions involving the first three pairs of valence subbands (V1, V2, V3) and the first pair of conduction subbands (C1). The solid and dashed lines are for the polarization vector along the k_1 ($[1\bar{1}0]$) (parallel to the wire) and k_2 ($[110]$) (perpendicular to the wire) directions. We found for the parallel polarization (solid lines), the squared optical matrix element for the V1-C1 transition has a maximum at the zone center with a value near 20 eV and remains close to this value for all finite k_2 and for $k_1 < 0.01(2\pi/a)$. For k_1 from 0.01 to $0.02(2\pi/a)$, it drops very quickly as a result of band mixing with lower valence subbands. For the perpendicular polarization, the optical strength for the V1-C1 transition is nearly zero for finite k_2 and $k_1 = 0$. It gradually increases as k_1 increases and become appreciable for $k_1 > 0.02(2\pi/a)$. This means that the bond orbitals involved in the V1 subband states are mostly x' -like. This is consistent with the consequence of the lateral confinement on a HH1-like quantum well state (see discussions in Ref. 9). Comparing Fig. 10 with Fig. 8, we see that for the V1-C1 transition not only the optical anisotropy is reversed, but their k_1 dependence is also qualitatively different. In Fig. 8, the optical strength for the C1-V1 transition decays very slowly as k_1 increases, showing no sign of band-mixing effect, consistent with the absence of anti-crossing pattern in Fig. 7.

To calculate the optical anisotropy in the photoluminescence spectra, we integrate the squared optical matrix element over the range of k_1 corresponding to the spread of exciton envelope function in the k_1 space. The exciton envelope function is obtained by solving the 1D Schrödinger equation for the exciton in the effective-mass approximation similar to what we did in Ref. 9. The exciton binding energy obtained is 23 meV. We found that the ratio of the averaged optical strength for the V1-C1 transition for the parallel to perpendicular component of the polarization vector is 0.5 and 3.82 for the model structures 1 and 2 considered here. Our results for QWR model structure 2 are qualitatively similar to that reported in Ref. 9 for a QWR structure made of 3D alloy structures with composition modulation. Here we have a 2D alloy structure with composition modulation and a SPS structure in the third direction. Furthermore, we have included the effects of microscopic strain distribution at the atomistic level. The agreement with the experimental observation for the band gap (735 meV) and ratio of parallel to perpendicular optical strength (around 2 - 4 for a number of QWR structures)[1,2] is also much better than that obtained in the 3D alloy structure model. Thus, we

conclude that our model structure 2 has captured all the essential features of the realistic experimental SILO QWR structure.

IV. SUMMARY

We have calculated the band structures and optical matrix elements for the strained GaInAs QWR grown by the SILO method. The actual SPS structure and the microscopic strain distribution has been taken into account. The effects of microscopic strain distribution on the valence subband structures and optical matrix elements are discussed for two model SILO QWR structures, one with ideal periodicity along the wire axis and abrupt changes of In composition in the lateral direction, while the other with a 2D alloy mixing and gradual lateral modulation of the In composition in the interface layers of the SPS structure. The valence force field (VFF) model is used to calculate the equilibrium atomic positions in the model QWR structures. This allows the calculation of the strain distribution at the atomistic level.

We found that in model structure 1 or any similar structures with ideal periodicity along the wire axis, the strain distribution always has large off-diagonal (shear strain) components, which can alter the valence subband structures substantially and give rise to a reversed optical anisotropy compared with QWR structures with negligible shear strain (such as the model structure 2). This points to a possibility of "shear strain-engineering" to obtain QWR laser structures of desired optical anisotropy.

The band gap and optical anisotropy obtained for model structure 2 are in very good agreement with experimental observations on most InGaAs SILO QWRs with similar specifications. This indicates that our model structure 2 is fairly close to the realistic structure at least in the essential physical aspects. The optical anisotropy obtained in our model structure 1 is reversed compared with that in model structure 2 and in the photoluminescence measurements for most InAs/GaAs SILO QWRs. However, there exist a few InAs/GaAs SILO QWR samples which display the reversed optical anisotropy at 77 K.[23] Furthermore, strained InAs/GaAs QWRs with ideal periodicity along the $[1\bar{1}0]$ axis may be grown via e-beam lithography followed by *in situ* regrowth. It will be interesting to see if these ideal QWR structures grown in the future will display the reversed optical anisotropy as we predicted here.

ACKNOWLEDGEMENTS

This work was supported in part by the National Science Foundation (NSF) under Grant No. NSF-ECS96-17153. J. S. was also supported by a subcontract from the University of Southern California under the MURI program, AFOSR, Contract No. F49620-98-1-0474. We would like to thank K. Y. Cheng and D. E. Wohlert for fruitful discussions and for providing us with the detailed experimental data of the QWR structures considered here.

-
- ¹ S.T. Chou, K. Y. Cheng, L. J. Chou, and K. C. Hsieh, Appl. Phys. Lett. **17**, 2220 (1995); J. Appl. Phys. **78** 6270, (1995); J. Vac. Sci. Tech. B **13**, 650 (1995); K. Y. Cheng, K. C. Hsien, and J. N. Baillargeon, Appl. Phys. Lett. **60**, 2892 (1992).
- ² D. E. Wohlert, S. T. Chou, A. C. Chen, K. Y. Cheng, and K. C. Hsieh, Appl. Phys. Lett. **17**, 2386 (1996).
- ³ Y. Tang, H. T. Lin, D. H. Rich, P. Colter and S. M. Vernon, Phys. Rev. **53B** R10501, (1996).
- ⁴ J. W. Matthews and A. E. Blakeslee, J. Cryst. Growth **27**, 18 (1974).
- ⁵ P. L. Gourley, J. P. Hohimer, and R. M. Biefeld, Appl. Phys. Lett. **47**, 552 (1985).
- ⁶ A. R. Adams, Electron. Lett. **22**, 249 (1986).
- ⁷ E. Yablonovitch and E. O. Kane. IEEE J. Lightwave Technol. LT-4, 504 (1986).
- ⁸ G. P. Agrawa and N. K. Dutta, Long Wavelength Semiconductor Lasers, 2nd ed. (Van. Nostrand Reinhold, New York, 1993) Chap.7.
- ⁹ L. X. Li and Y. C. Chang, J. Appl. Phys. **84** 6162, 1998.
- ¹⁰ H. Jiang and J. Singh, Phys. Rev. **B56**, 4696(1997).
- ¹¹ R. M. Martin, Phys. Rev. **B1**, 4005(1969).
- ¹² P. N. Keating, Phys. Rev. **145**, 637(1966).
- ¹³ Y. C. Chang, Phys. Rev. **B37**, 8215 (1988).
- ¹⁴ Mau-Phon Houg and Y.C Chang, J. Appl. Phys. **65**, 3096 (1989).
- ¹⁵ M.A.Cusack, P.R. Briddon, and M. Jaros, Phys. Rev. **B56**, 4047(1997).
- ¹⁶ G. L. Bir and G. E. Pikus, Symmetry and Strain Induced Effects in Semiconductors (Halsted, United Kingdom, 1974); L.D. Landau and E. L. Lifshitz, Theory of Elasticity (Addison-Wesley Publishing Company Inc, Reading, Massachusetts, USA, 1970).
- ¹⁷ M. Podgorny, M.T. Czyzyk, A. Balzarotti, P. Letordi, N. Motta, A. Kisiel, and M. Zimmel-Starnawska, Solid State Comm. **55**, 413(1985).
- ¹⁸ C. Pryor, J. Kim, L.W. Wang, A.J. Williamson and A. Zunger, Phys. Rev. **B183**, 2548(1998).
- ¹⁹ S. Adachi, J. Appl. Phys. **53**, 8775 (1982).

- ²⁰ H. Mathieu, P. Meroe, E. L. Amerziane, B. Archilla, J. Camassel, and G. Poiblaud, Phys. Rev. B **19**, 2209 (1979); S. Adachi and C. Hamaguchi, Phys. Rev. B **19**, 938 (1979).
- ²¹ J. M. Hinckley and J. Singh, Phys. Rev. B **42**, 3546 (1990).
- ²² O. Madelung and M. Schulz, Landolt-Borstein (1982).
- ²³ M. Razeghi, Ph. Maurel, F. Omnes, and J. Nagle, Appl. Phys. Lett. **51**, 2216 (1987).
- ²⁴ D.E. Wohlert, and K. Y. Cheng, private communications.
- ²⁵ G. D. Sanders and Y. C. Chang, Phys. Rev. B **31**, 6892 (1985).
- ²⁶ G. D. Sanders and Y. C. Chang, Phys. Rev. B **45**, 9202 (1992).

Figure Captions

Fig. 1. Schematic sketch of the basic (2,2) SPS segment in the SILO quantum wire for two model structures considered in the present paper. Each segment consists of four diatomic layers with 72 bulk unit cells in each layers. In structure 1, 29 Ga atoms in layer 1 are inter-changed with 29 In atoms in layer 3 so that the supercell is divided into two regions with the left being Ga-rich (region A) and the right being In-rich (region B). In structure 2, the first layer and third layer consist of 2D alloy structure with lateral modulation of the In composition as shown in the profile below. The 2D alloy structure models the mixing of Ga and In atoms during crystal growth when Ga or In islands of 0.4 monolayer are present.

Fig. 2. Diagonal strain distribution of the first SILO QWR structure [corresponding to Fig. 1(a)] in rotated frame. Dotted: $\epsilon_{x'x'}$. Solid: $\epsilon_{y'y'}$. Dashed: ϵ_{zz} .

Fig. 3. Off-diagonal strain distribution of the first SILO QWR structure [corresponding to Fig. 1(a)] in original frame. Solid: e_{xy} . Dashed: e_{xz} Dotted: e_{yz} .

Fig. 4. Diagonal strain distribution of the second SILO QWR structure [corresponding to Fig. 1(b)] in rotated frame. Dotted: $\epsilon_{x'x'}$. Solid: $\epsilon_{y'y'}$. Dashed: $\epsilon_{z'z'}$.

Fig. 5. Off-diagonal strain distribution of the second SILO QWR structure [corresponding to Fig. 1(b)] in original frame. Solid: e_{xy} . Dashed: e_{xz} Dotted: e_{yz} .

Fig. 6. Conduction and valence band edges of the constituent materials for two SILO QWR structures with and without the effect of strain as functions of the [110] coordinate y' . Solid lines are for unstrained SPS structure, dashed lines are for the SPS structure under the same y' -dependent strain distribution as in the corresponding SILO QWR structure, and dash-dotted lines are for 8 stacks of SPS structures sandwiched between $60\text{\AA}\text{Al}_{0.24}\text{Ga}_{0.24}\text{In}_{0.52}\text{As}$ barriers including the QWR strain distribution.

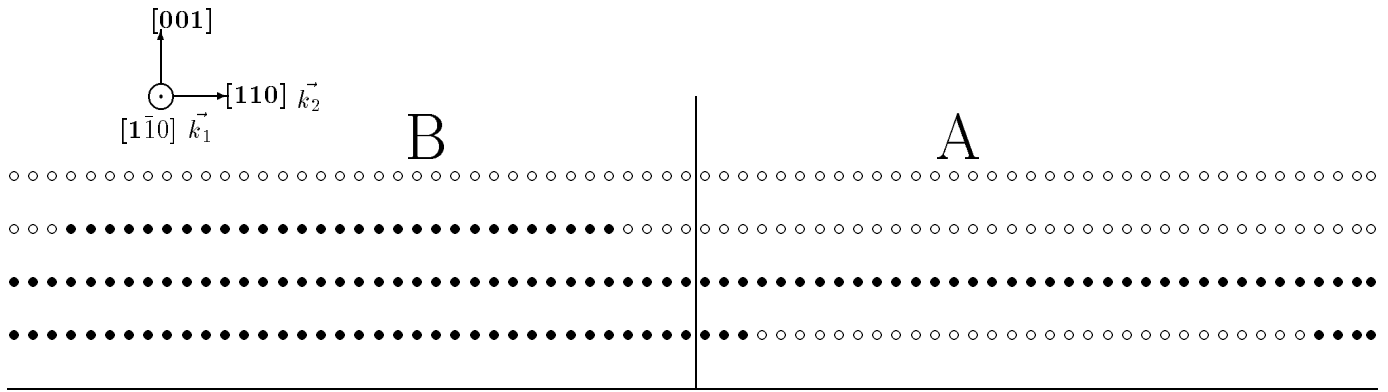
Fig. 7. Valance subband structures for the SILO QWR structures depicted in Fig. 1(a).

Fig. 8. Squared optical matrix elements for transitions from the top three pairs of valence subbands to the first pair of conduction subband for light polarized parallel (solid) and perpendicular (dashed) to the QWR axis for the SILO QWR structure depicted in Fig. 1(a).

Fig. 9. Valance subband structures for the SILO QWR structure depicted in Fig. 1(b).

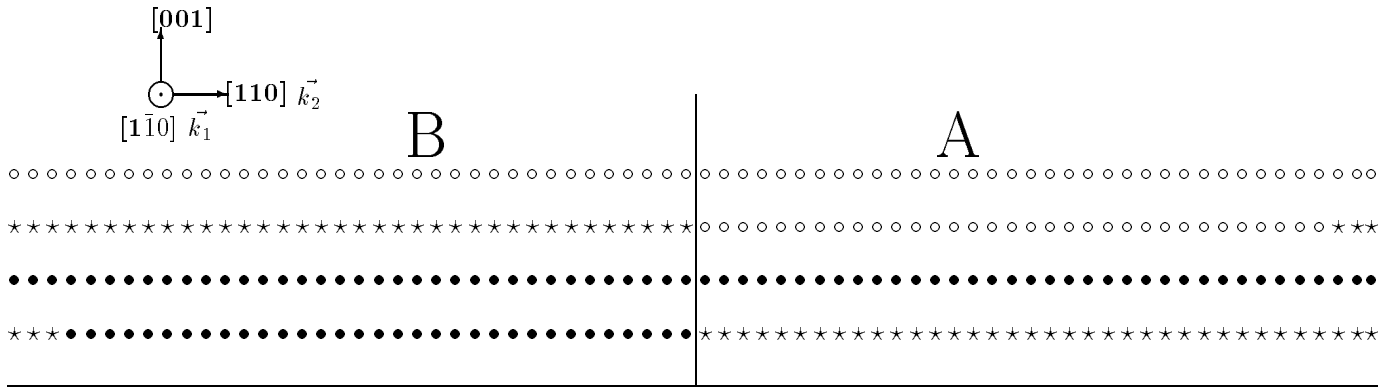
Fig. 10. Squared optical matrix elements for transitions from the top three pairs of valence subbands to the first pair of conduction subband for light polarized parallel (solid) and perpendicular (dashed) to the QWR axis for the SILO QWR structure depicted in Fig. 1(b).

(a)



○ ○ ○ ○ ○ In layer, and ● ● ● ● ● Ga layer.

(b)



○ ○ ○ ○ ○ In layer, ● ● ● ● ● Ga layer, and ★ ★ ★ ★ ★ alloy layer.